energies

MDPI

Article

Experimental Study on Heat Recovery in a $CaO/Ca(OH)_2$-Based Mechanical Fluidized Bed Thermochemical Energy Storage Reactor

Viktor Kühl [1,*], Marc Linder [2] and Matthias Schmidt [1]

[1] German Aerospace Center (DLR e.V.), Institute of Engineering Thermodynamics, Linder Höhe, 51147 Cologne, Germany; matthias.schmidt@dlr.de
[2] German Aerospace Center (DLR e.V.), Institute of Engineering Thermodynamics, Pfaffenwaldring 38-40, 70569 Stuttgart, Germany; marc.linder@dlr.de
* Correspondence: viktor.kuehl@dlr.de

Abstract: Long-term storage of seasonally available solar energy and its provision to balance heating energy demand can contribute significantly to the sustainable use of energy resources. Thermochemical energy storage is a suitable process for this purpose, offering the possibility of loss-free long-term energy storing and heat supply. In order to develop suitable technical solutions for the use of this technology, novel reactor concepts and scientific questions regarding material and technology development are being investigated. In this publication, the energy storage process of a long-term energy storage system based on a ploughshare reactor is experimentally investigated under various technically relevant operating conditions. One specific aspect of this technology is related to the release of water vapour during the charging process. Therefore, this work focusses, in particular, on the possibility of technically utilizing the latent heat of the released water vapour in the range of 45 °C to 80 °C, which covers the operating requirements of common heating systems in households. The experiments have shown that the dehydration process enables the separation of two heat fluxes: the chemically bound energy for long-term storage and the physically (sensible and latent) stored energy for short-term applications. However, the limitation of gas transport was also identified as the most important influencing parameter for optimising the performance of the process.

Keywords: thermochemical energy storage; calcium oxide/hydroxide; mechanically fluidized bed reactor; latent heat recovery; long-term energy storage; renewable heating

Citation: Kühl, V.; Linder, M.; Schmidt, M. Experimental Study on Heat Recovery in a $CaO/Ca(OH)_2$-Based Mechanical Fluidized Bed Thermochemical Energy Storage Reactor. *Energies* **2024**, *17*, 4770. https://doi.org/10.3390/en17194770

Academic Editors: Chunrong Zhao and Jianyong Wang

Received: 21 August 2024
Revised: 7 September 2024
Accepted: 11 September 2024
Published: 24 September 2024

1. Introduction

In the northern countries, a significant proportion of fossil fuels is employed for the purpose of heating residential properties during the winter months. In the European Union, for instance, this proportion accounts for approximately two-thirds of the residential sector's final energy consumption [1]. Eurostat [2] indicates that a sufficient quantity of renewable energy is available on an annual average to satisfy this demand. The implementation of cost-effective energy storage solutions would lead to a notable reduction in the reliance on fossil fuels in this sector. Long-term storage systems offer this possibility.

Various energy storage technologies based on adsorption, absorption, or chemical reactions are summarised as thermochemical storage, which can cover a wide range of applications for the utilisation of renewable heat due to their temperature range and energy density [3].

Based on fundamental studies on the material [4–7], quicklime-based storage systems have been investigated as possible candidates for cost-effective, loss-free energy storage. Extensive work has already been carried out to shed light on aspects such as fundamental thermodynamics [8,9], system integration [10], and the techno-economic aspects of the technology [11].

The $Ca(OH)_2 \rightleftharpoons CaO + H_2O$ reaction system has been identified as a promising material for the storage of chemical energy. The material has a high energy density of up to 215 kWh/m^3 [10]. Furthermore, as part of the technical lime cycle, the material is inexpensive and available in large quantities. In recent years, a variety of concepts have been developed for the utilisation of lime as an energy storage medium. As outlined by Wang et al. [12], three distinct reactor concepts have emerged. In addition to fixed-bed reactors, which are only used for basic research under laboratory conditions due to the limited possibilities for upscaling, there are also moving-bed reactors with the advantage of a continuous operation mode [13] and fluidized-bed reactors where a batch [14,15] as well as a continuous operation mode is known [16]. However, both concepts require the storage material to possess specific properties in terms of fluidisability and material feed. These systems are intended for industrial processes, as the technical complexity of these systems prevents their use for residential purposes.

A further concept known as mechanical-induced fluidization combines the advantages of fluidisation and of using unmodified material, see Risthaus et al. [17]. In this setup, the heat transfer is significantly enhanced by fluidisation, while the reactor can be operated in batch mode with unmodified powder material. The smaller effective heat transfer surface within the reaction zone, in comparison to the aforementioned fixed bed reactors, is counteracted here by the principle of mechanical fluidisation. The material is fluidised using a ploughshare mixer, which maintains its movement continuously. This approach addresses two significant challenges associated with unmodified powder material: the low thermal conductivity of the powder and its tendency to agglomerate. Theoretically, heat transfer coefficients of up to 350 W/m^{2}K can be achieved [17].

The general functional principle of lime-based thermochemical energy storage, particularly for domestic heat supply, is described in detail by Schmidt et al. [10]. Summarising, electrical energy from grid surpluses that arise in connection with seasonal or short-term energy overproduction is used to provide heat at a temperature level of 500–550 °C and to allow a chemical reaction to take place. Theoretically, at the dehydration of $Ca(OH)_2$, around 40% of the supplied energy is converted in the form of reaction enthalpy of the produced CaO, which is a material property and can therefore remain constant for an unlimited time period. So if the material is prevented from further reaction, the energy can be stored for extended periods with minimum heat loss at ambient conditions [18]. The release of energy in the form of heat is the result of an exothermic reaction of the material with H_2O.

The studies demonstrate that only a portion of the energy can be stored for long-term requirements. As a by-product of the energy-storing process, a further significant quantity of heat is turned into the form of latent and sensible heat of the produced water vapour. This heat must either be utilised immediately or stored in short-term facilities. The aforementioned concept would therefore be particularly suitable for consumers or processes that combine a base-load heat demand, a superimposed strong seasonal heat demand, and an opposite seasonal energy surplus. During periods of sufficient energy availability, the material would be charged, and the released latent and sensible heat would satisfy the base-load demand. In periods of insufficient energy availability, the chemically bonded energy can be released to meet the additional demand. The fundamental possibility to recover especially the latent energy released from this reactor type is still questionable due to the difficulties with gas–solid separation, as described by Risthaus et al. [17].

Its low efficiency is regarded as the primary drawback of thermochemical storage technology, which ultimately renders it unfeasible from a commercial standpoint, see Abedin et al. [19]. It is therefore important to ensure that the latent and sensible heat is actually available for short-term energy supply in order to make the entire process effective. This work demonstrates, through experimental investigation, the potential for utilising the latent heat generated during the reaction, as it would increase the total efficiency of the thermochemical storing process [10]. As part of the study, the reactor design was adapted to enable operational procedures pertinent to the intended application to be carried out. The

resulting data permitted the determination of a number of properties, including pressures, temperatures, filter permeability, conversion rates, and performance. The data obtained from this study may thus be used as a basis for the validation of numerical models for the operational strategies of long-term energy storage systems and their incorporation into existing energy supply systems [20,21].

2. Materials and Methods

The investigation employs a commercial $Ca(OH)_2$ powder material, procured from Rheinkalk GmbH/Lhoist group. The analysis of the material indicates a bulk density of 380 kg/m^3, a mean particle diameter (d_{50}) of 5.1 µm, and a specific surface area of 18 m^2/g. To ensure the initial conditions are consistent, a fresh batch of material is used for each test run, and the reactor is completely emptied after each test. To verify the initial material composition, thermogravimetric analysis (TGA) measurements are performed on the supplied batches. Two batches with slightly different compositions are used for the investigation. The average composition of the material is calculated to be $Ca(OH)_2$: 88%; CaO: 5%; $CaCO_3$: 7%. The average material loading quantity into the reactor is approximately 4967 ± 76 g.

2.1. Test Bench

The main components and operational principles of the test bench used in the present study are described in the work of Risthaus et al. [17]. The configuration has been adapted for the investigation described in this work, and the essential features of the current test bench configuration are described in the following paragraphs.

The test setup consists of three principal components: the reactor unit, the vacuum, and the condenser unit. The reactor is insulated with a thermal material. The reactor is furnished with five principal heating wires, which are wrapped around the reactor wall and constitute discrete heating zones along the reactor's length. The maximum output heating power for each heating zone is 4.7 kW, as illustrated in Figure 1 ②. Additional support heating wires with a power of 1 kW are positioned at the flanges, the clutch, and the pressure sensor supply lines. The aforementioned elements are employed to minimise heat loss and prevent condensation on the colder surfaces, respectively. The transfer of energy occurs via the reactor wall, as illustrated in Figure 1 ①. The reactor has an inner length of 50 cm, a diameter of 20 cm, and a capacity of approximately 5 kg $Ca(OH)_2$ material. A rotating ploughshare mixing tool, as illustrated in Figure 1 ③, is installed within the reactor to provide mechanical fluidisation. The reactor is airtight and can be operated at temperatures of up to 520 °C and a pressure range of 0 to 240 kPa_{abs}. It is only operated as a closed, airtight system.

The reactor is connected to the condenser component via a heated steam hose. During the operational phase, the produced $H_2O_{(g)}$ is driven in the direction of the condenser unit due to the naturally occurring pressure gradient. In order to separate the solid and gas phases, a filter unit is installed on the inner side of the front flange, as illustrated in Figure 1 ④. In a previous investigation, the presence of a filter cake material layer on the filter surface was observed, which resulted in a limitation of the mass flow and, consequently, the reactor power [17]. Accordingly, the filter construction has been modified with the objective of enhancing the mass flow through the filter surface, as illustrated in Figure 2. A static filter holder has been installed between the reactor flange and the reactor lid. The filtration process is achieved through the use of a clamped stainless-steel filter mesh, created through a twill weave with a geometric opening of 10 µm. In order to maintain the filter surface in a state free from deposits, a rotating cutting tool is connected to the rotating ploughshare and positioned in front of the filter surface, with the function of permanently removing deposits. The distance between the cutting tool and the filter surface is set in consideration of the expected thermal expansion of the material. The dimensions of the filter are as follows: inner radius: 36 mm, outer radius: 81,5 mm, resulting in a filtering surface of A_F: 0.0168 m^2. The impact of this new design is presented in the results section.

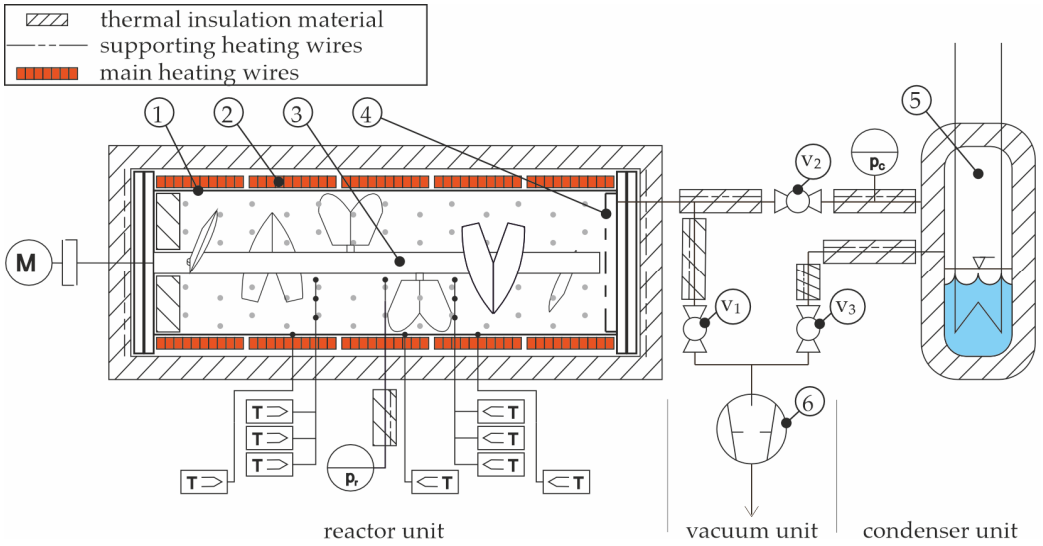

Figure 1. The schematic drawing of the storage system illustrates the main components utilized for the experimental study. ① Reactor wall, ② main heating wires used as primary energy source for dehydration process, ③ ploughshare tool, ④ filtering unit for gas/solid separation, ⑤ condenser unit as heat and pressure sink, ⑥ vacuum pump, v1–v3 valves, p—pressure sensors, T temperature sensors.

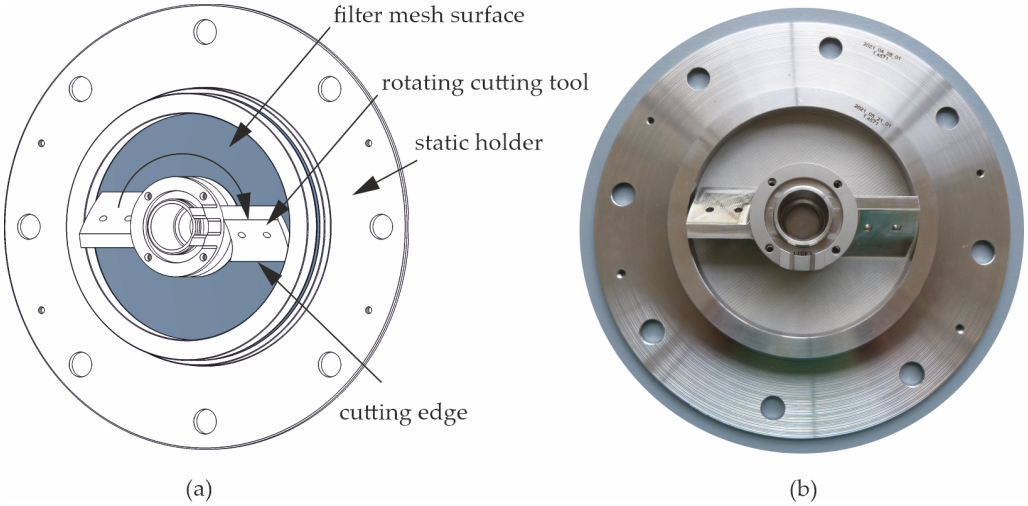

Figure 2. Filtering unit illustration of components (**a**) and final product (**b**).

The main component of the test bench used to measure the actual conversion is the condenser unit, as illustrated in Figure 1 ⑤. The condenser unit has a cooling power of 10 kW and a water tempering capacity. The apparatus is capable of functioning at temperatures between 10 °C and 100 °C and a pressure range from 0 kPa_{abs} to 240 kPa_{abs}. The vacuum unit consists of heated water vapour supply lines, electrical or manually operated valves (v_1, v_2, v_3), and a Busch R5 RA 0025 F vacuum pump, Figure 1 ⑥, which is capable of providing a minimum pressure of 0.01 kPa_{abs}.

2.2. Measuring Technics

Pressure measurements are performed utilising Keller PAA-35XHTT pressure sensors, KELLER Druckmesstechnik AG, 8404 Winterthur, Switzerland, which have a range of 0 kPa_{abs} to 300 kPa_{abs} and a maximum error of ±0.6 kPa. Two pressure sensors are installed: one in the reactor (p_r, Figure 3) and the other in proximity to the condenser unit (p_c, Figure 1). To prevent condensation within the feed line, the reactor pressure feed line is heated externally to 100 °C. The p_r feed line comprises a steel pipe with an inner diameter

of 2 mm. To prevent material accumulation and blockage of the feed line, filter material is welded to the front surface of the pipe, see Figure 3.

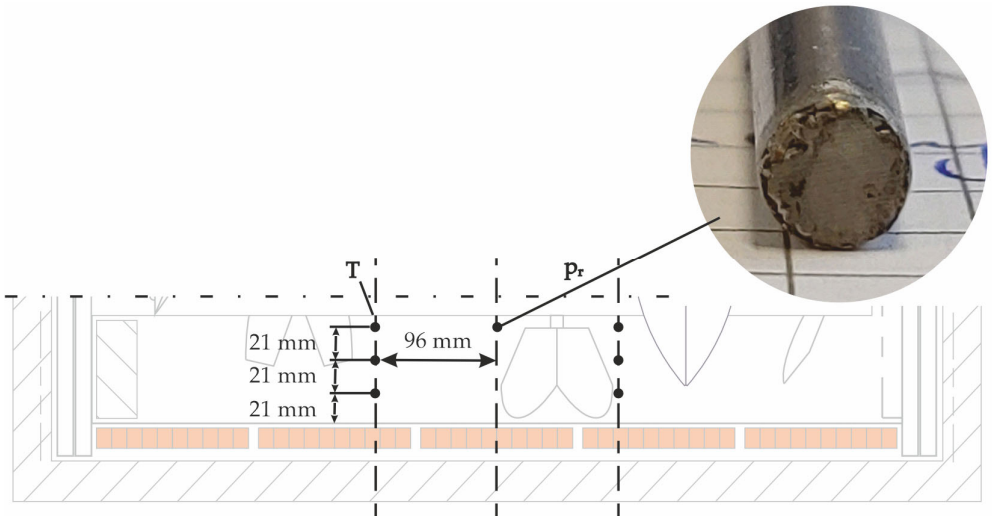

Figure 3. Detailed illustration of position of the main temperature and pressure sensors and of the pressure feeding line cover.

The temperature measurements are performed utilising Ø 0.5 mm type K class 1 thermocouples. Three-point type K thermocouples with a diameter of 4 mm are utilised for the determination of the bulk material temperature. The sensor positions are illustrated in Figure 3.

As the system is closed and all the total produced water vapour is condensed in the condenser, the condenser filling level is a direct method of determining the conversion and reactor performance. The condenser filling level (F) is measured by a microwave level sensor Vegaflex 65, VEGA Austria GmbH, 4050 Traun, Austria, with an uncertainty of ±2 mm.

The equilibrium condition of temperature and pressure in the condenser can be described using the Magnus formula.

$$E_w(T) = 6.112\ \text{hPa} \times \exp\left(\frac{17.5 \times T}{241.2\ ^\circ\text{C} + T}\right) \quad (1)$$

The equilibrium formula proposed by Schaube et al. [5] is used to describe the reaction equilibrium within the reactor.

$$\ln\left(\frac{p_{EQ}}{10^5}\right) = -\frac{12845}{T_{EQ}} + 16.508 \quad (2)$$

The conversion of the reactants is defined by the following equation:

$$X_i = \frac{n_i}{n_{i,0}} \quad (3)$$

In order to gain a more representative overview, it is sufficient to consider only the change in the CaO. Adopting the assumption of a closed system and considering the relationship $X_{CaO} = X_{H2O} = 1 - X_{Ca(OH)2}$, the value of X_{CaO} can be calculated using the following equation:

$$X_{CaO} = \frac{\Delta F \times A_{condenser} \times \rho_{H_2O} \times M_{Ca(OH)_2}}{M_{H_2O} \times m_{Ca(OH)_2,0}} \quad (4)$$

The latent heat energy, also referred to as latent heat, is derived from the measurement of the change in condenser filling level and is calculated using the following equation:

$$\dot{Q}_{latent} = \frac{\Delta F \times A_{condenser} \times \rho_{H_2O} \times \Delta H_{vap}}{M_{H_2O} \times \Delta t} \quad (5)$$

The combined permeability of the filter material and the deposit on the filter is derived from Darcy's law and determined by the following equation:

$$K = \frac{\dot{V} \times \eta \times l}{A_{filter} \times \Delta p} \quad (6)$$

2.3. Test Procedure

The principal focus of this investigation is to determine the feasibility of recovering latent heat during the dehydration process. Accordingly, the reactor is operated in the dehydration mode only. In order to achieve equal test conditions, the test procedure is standardised. It can be subdivided into the following process steps: loading, preheating, evacuating, reaching initial conditions, reaction start, steady state, reaction end, and venting. These are described in further detail below. The expected temperature, pressure, and conversion profiles are shown in Figure 4. Test procedure: phases, expected profiles of p, T, X, and activation of valves and vac. pump during the dehydration process are illustrated. The grey area marks the time range of the steady state, which was considered for the calculations. Black bars show the active period (ON/OPEN).

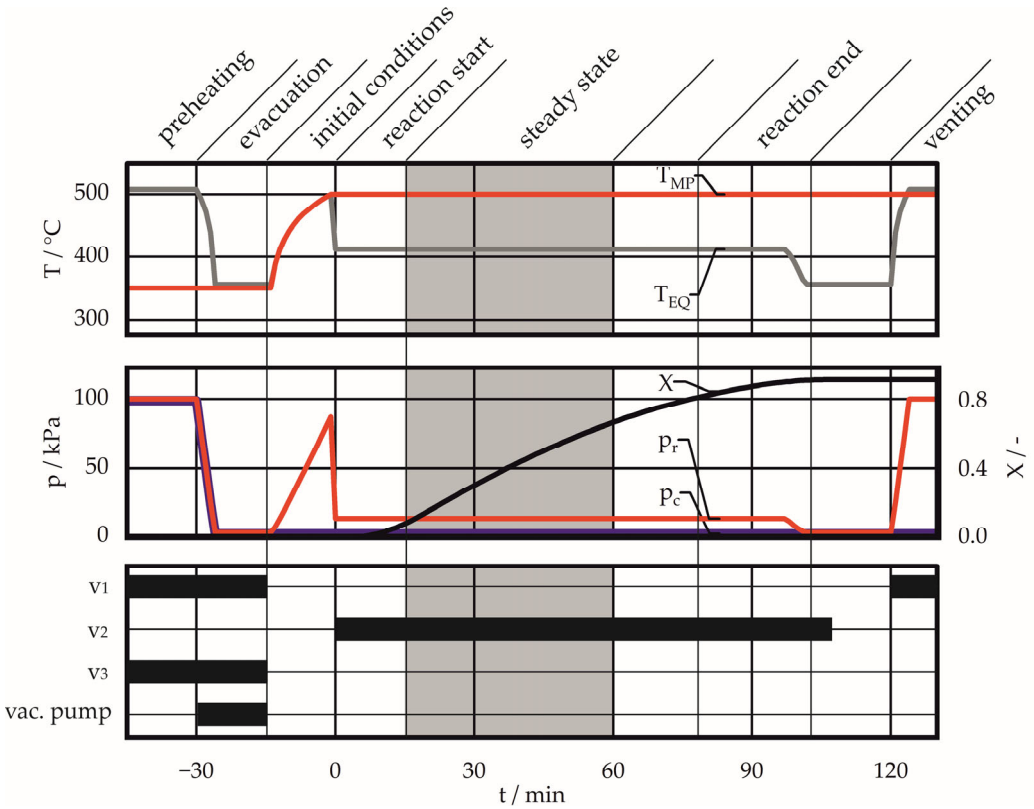

Figure 4. Test procedure: phases, expected profiles of p, T, X, and activation of valves and vac. pump during the dehydration process are illustrated. The grey area marks the time range of the steady state, which was considered for the calculations. ON/OPEN mark the active period.

Loading ($t \leq -45$): A quantity of approximately 5 kg of $Ca(OH)_2$ material is manually loaded into the reactor. At this time, the temperature of the material and the reactor are at

ambient temperature. The initial weight and composition of the material are determined. The filter surface is cleaned of all deposits. The cutting tool is cleaned of all deposits and adjusted so that free rotation is ensured.

Pre-heating ($-45 \leq t \leq -30$): The reactor is preheated to a temperature of approximately 350 °C, while the condenser is simultaneously preheated to its initial temperature. The ploughshare mixing tool is rotating at a frequency of 250 rpm. During this phase, the condenser and reactor are connected to the environment (v_1, v_3 open, vacuum pump off), yet separated from each other (v_2 closed). This configuration is maintained for approximately 15 min to ensure that the conditions remain in a steady state.

Evacuating ($-30 \leq t \leq -15$): The vacuum pump is connected to generate vacuum conditions in both the reactor and the condenser. This ensures the lowest possible concentration of inert gas in the system, which could disrupt the condensation process. Once the minimum pressure is reached, valves v_1 and v_3 are closed. At $t = -15$, the required test temperature of the reactor is set.

Reaction ($0 \leq t \leq 90$): The reaction starts, resulting in an increase in pressure within the reactor until a steady state is reached. Once the initial conditions have been reached, the reactor and the condenser are connected (v_2 open, $t = 0$). A pressure drop occurs in the reactor, which is followed by condensation in the condenser. This reduces the pressure, prompting the reaction in the reactor to produce more vapour in order to maintain equilibrium. This results in a dynamic balance state within the system, accompanied by a mass flow to the condenser. From this point onwards ($15 \leq t \leq 60$), the reaction proceeds continuously, with the change in water level indicating a linear conversion progression. Once a critical quantity of $Ca(OH)_2$ has been converted, the equilibrium cannot be maintained, and the reactor pressure tends towards the corresponding pressure in the condenser. At this point, the conversion has reached its final level ($t = 100$).

End of experiment ($t > 100$): Following a minimum period of 120 min, the heating wires are deactivated, the reactor and the condenser are separated (close v_2), and the reactor is vented via v_1 ($t = 120$). After the reactor has cooled down to 350 °C, the front reactor flange is opened, and a material sample is taken for further TGA analysis.

2.4. Measurement Matrix

Figure 5 illustrates the operational ranges of the system. The anticipated pressures and temperatures in the reactor and condenser units are predominantly constrained by their working media characteristics. Given that the experimental conditions are analogous to those of pure water vapour atmosphere, the temperature and pressure within the reactor and condenser can be modelled using equilibrium conditions for vaporisation and the $Ca(OH)_2 \rightleftharpoons CaO + H_2O$ reaction, respectively, see Figure 5 solid lines.

In order to ensure optimal technical conditions for the duration of the measurement campaign, the temperature of the reactor core has been restricted to a maximum of 500 °C, while the condenser cooling limit is approximately 10 °C. These boundary conditions must also be considered (Figure 5, stitch dotted lines). In order to ensure a reaction, it is essential to guarantee vapour mass transport, which necessitates a pressure drop between the operating point of the reactor (OPr) and the operating point of the condenser (OPc), (Figure 5, dots).

The measurement matrix (Table 1) was designed with consideration of potential system applications and operational conditions. As the reactor forms part of a thermochemical heat storage system, with domestic heating applications being the primary focus, the test points were derived from the typical heating circuit inlet temperatures, which range from 70–90 °C for radiator heaters in old buildings, 50–70 °C for radiator heaters in newer standards buildings, and 35–45 °C for underfloor heating systems. Furthermore, a condensation at 10 °C was used to investigate the system under conditions of minimum water vapour pressure, which can be realised in the set-up. The condenser water temperature and $Ca(OH)_2$ core temperature are suitable as potential control values. After considering all

parameters, the selected set points are 10 °C, 45 °C, and 80 °C on the condenser and 430 °C, 470 °C, and 500 °C on the reactor side, as illustrated in Figure 5 (dots).

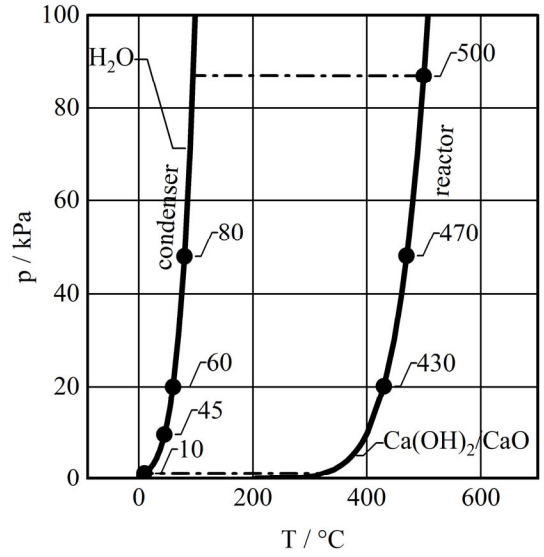

Figure 5. System boundary conditions.

Table 1. Measurement matrix.

Run	Initial Material Mass	Initial Material Composition $Ca(OH)_2/CaO/CaCO_3$	Setpoint Temperature Reactor/Condenser
[#]	[kg]	[%]	[°C]
009	5.0	91.25/5.93/2.82	500/10
010	5.0	86.67/4.43/8.90	500/10
011	5.1	86.67/4.43/8.90	470/10
012	4.9	86.67/4.43/8.90	430/10
014	4.9	86.67/4.43/8.90	500/45
015	5.0	86.67/4.43/8.90	500/60
016	4.9	86.67/4.43/8.90	500/80
020	5.0	91.25/5.93/2.82	470/45
021	5.0	91.25/5.93/2.82	470/60

3. Results and Discussion

3.1. Filtering Modification

One significant aspect of this study was the investigation of the impact of the filter design. As part of the investigation, the prototype filter setup has been redesigned, as described in Section 2.1, with the objective of reducing the deposits in front of the filter and enabling a higher water vapour mass flow. In order to evaluate the functionality, two tests were conducted under identical operational parameters. While run009 was executed without the cutting tool, run010 employed the cutting tool. Figure 6 illustrates the temperature, pressure, and conversion data during the tests. Although the reaction conditions for both experiments should be identical, a slight decrease in reactor pressure (p_r) is evident towards the end of the experiment in run009. However, the most evident discrepancy is the calculated conversion, which demonstrates a significantly higher ratio in run010. It can be observed that the reactor pressure of run010 declines at t = 70 min, while the conversion reaches its maximum value asymptotically towards the conclusion of the experiment. The final conversion value is approximately 0.91. It is evident that at time t = 70 min the mass flow towards the condenser exceeds the vapour production by the reaction, as indicated by the reducing pressure within the reactor. The reaction is ultimately completed, and no further conversion occurs after t = 110 min.

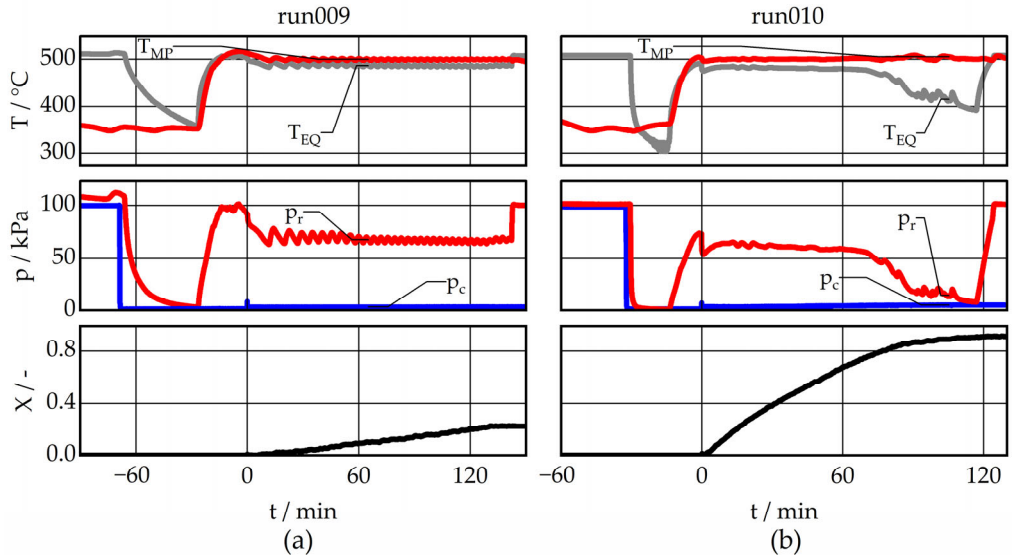

Figure 6. Filtering modification: performance comparison at 500/10 for a test without (**a**) and with the cutting tool (**b**).

In contrast, the conversion in run009 is notably slower, reaching a maximum value of 0.22 within the same experimental time range. This leads to the assumption that in this case the mass flow through the filter is significantly restricted. In other words, the pressure difference available for mass transport through the piping and filter is thermodynamically defined, but the filter "consumes" it already for a comparatively smaller mass flow rate. At the end of the tests, the reactor is ventilated. In both cases, the ambient pressure is reached rapidly.

Following the completion of both tests, a layer thickness measurement of the filter deposits was conducted. The deposits formed in run009 exhibited a solid layer with a thickness corresponding to the distance between the filter surface and the first rotating ploughshare mixing blade, as illustrated in Figure 7a,c. However, the thickness was reduced to 3 mm by the installation of the cutting tool, as illustrated in Figure 7b,d. The thick filter deposits, which were identified and described in earlier studies by Risthaus et al. [17] resulted in the limitation of operational conditions.

By modifying the filter configuration, the issue of restricted mass transfer could be sufficiently managed to enable the operational parameters to be adjusted to permit the processing of materials at lower temperatures. The complete conversion of the material to 90% CaO was achieved in a reasonable time of less than 120 min. A direct comparison of the tests with and without the built-in cutting tool demonstrates that the enhancement in mass transfer through the filter in this configuration results in a six-fold increase in the conversion rate, from 1.72×10^{-3} per minute for run009 to 1.02×10^{-2} per minute for run010. This allows for further investigation to be carried out with the objective of characterising the reactor operation.

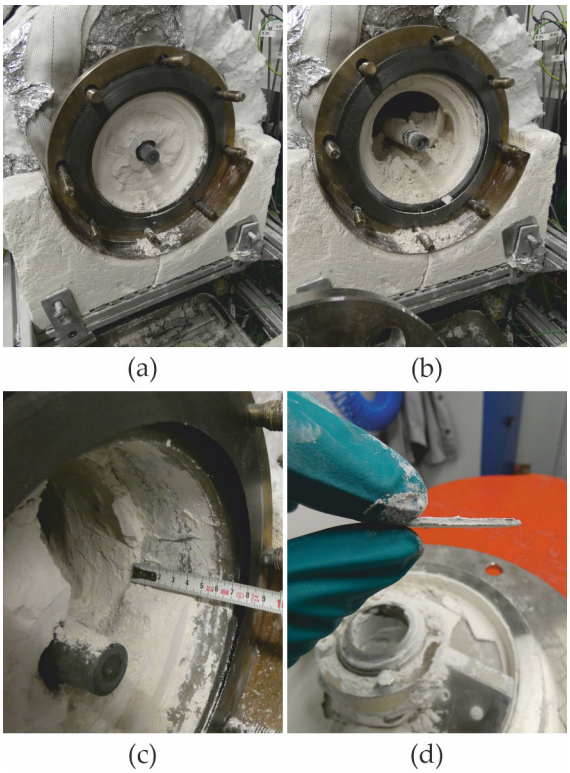

Figure 7. Filter cake formations comparison at 500/10 for a test without (**a**,**c**) and with the cutting tool (**b**,**d**).

3.2. System Performance

The objective of the study was to gather experimental data on the dehydration process in a ploughshare reactor in order to gain a deeper understanding of the potential for recovering latent energy released during the charging process. To this end, a series of systematic tests were conducted utilising the defined measurement matrix, as detailed in Table 1. For the purposes of this analysis, only the measurement data between t = 12 min and t = 60 min was considered, as it was assumed that conditions were almost stationary, thus enabling a more accurate comparison of the results.

3.2.1. Reactor Pressure

Figure 8 illustrates the equilibrium curve of $H_2O_{(l)} \rightleftharpoons H_2O_{(g)}$ (water vapour pressure curve) and the reaction equilibrium curve of $Ca(OH)_{2(s)} \rightleftharpoons CaO_{(s)} + H_2O_{(g)}$. These conditions are representative of those that can be expected in a pure water vapour atmosphere, as would be found in a condenser or reactor. The depicted points (OP_c, OP_r) present the experimental measured values. As can be observed, the measured values on the condenser side (H_2O) are in close alignment with the theoretical values. The mean deviation of all tests is 2.62 $\pm$ 0.53 kPa, which may be attributed to the presence of residual air in the system or measurement inaccuracies. In contrast, the measured values on the reactor side ($Ca(OH)_2/CaO$) indicate a pressure difference, with an average of -18.73 ± 4.44 kPa across all tests. This pressure difference represents a relevant parameter influencing the conversion ratio. However, the experimental data do not fully align with the kinetic equations, which was also observed by Risthaus et al. [17].

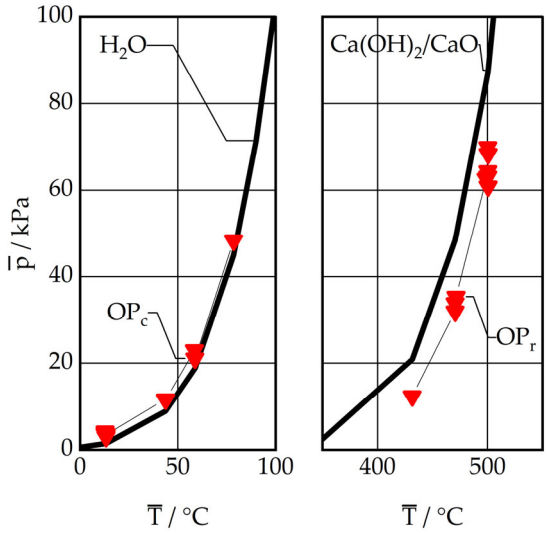

Figure 8. Reactor pressure deviation of condenser and reactor pressure measurements.

In order to gain a deeper insight into this discrepancy, a detailed examination was conducted on the pressure measurement. On the one hand, the possibility of blockage of the measuring supply line and condensation was excluded. The permeability of the supply line was evaluated prior to and following each experimental procedure. The supply lines were consistently heated above the condensation temperature. The rapid achievement of ambient pressure after system venting, as illustrated in Figure 6 suggests that the observed discrepancy is unlikely to be attributed to the pressure measurement. It can therefore be posited that the discrepancy may be attributed to the fact that, while the multipoint temperature measurement is an effective method for determining the average core temperature, it does not necessarily reflect the exact temperature of the entire material. It is possible that temperatures in the edge areas and deposit layers may be lower, which would result in an overall lower average temperature. An additional potential explanation may be associated with the existing dynamic balance state. In contrast to the fundamental investigations, which assume a static equilibrium, this investigation achieves a dynamic balance state in the reactor. To gain further insight into this phenomenon, the reactor was operated in a subsequent study without the condenser, thereby enabling the attainment of both static reaction equilibrium and approximate thermal equilibrium within the reactor. In accordance with the aforementioned conditions, the pressure and temperature state align with the theoretical equilibrium as postulated by Schaube et al. [5]. Consequently, it can be posited that the observed discrepancy is a consequence of a slightly lower average temperature within the reactor volume than that which was assumed on the basis of the multi-point core temperature measurement.

3.2.2. Operation Range Variation

Figure 9 illustrates the measured conversion from t = 0 min to t = 120 min for each test. For purposes of an improved overview, the diagrams were grouped according to setpoint temperature. The left-hand diagram depicts the experiments conducted with a reactor setpoint temperature of 500 °C, while the middle diagram illustrates the experiments carried out with 470 °C setpoint temperatures. In both cases, the condenser setpoint temperature is varied, thereby influencing the pressure within the condenser section. The diagram on the right illustrates the experiments conducted with varying reactor setpoint temperatures of 430/470/500 °C, while the condenser setpoint temperature was maintained at 10 °C, resulting in approximately equivalent pressure conditions within the condenser unit. It is evident that a latent heat recovery would be feasible under all operating conditions. The conversion curve shows a relatively constant course in the majority of cases, which suggests a homogeneous reaction process. However, there is an exception to this, namely

the 500/10 curve, where a decline in the conversion ratio can be observed after t > 70 min. This is due to the fact that the reaction is, under these conditions, already completed and the reactant in the form of $Ca(OH)_2$ is no longer available in sufficient quantities from this point onwards.

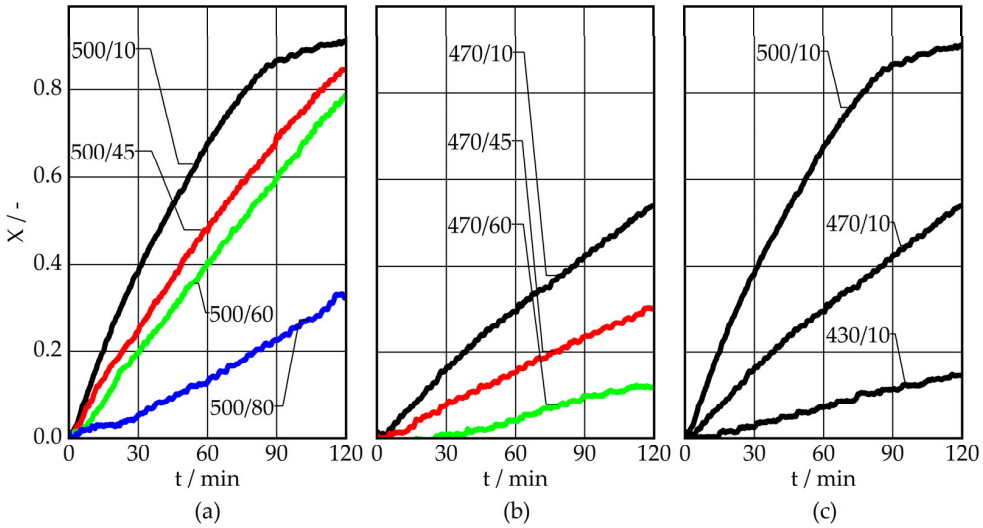

Figure 9. Conversion comparison for different operating conditions of 500 °C reactor temperature (**a**), 470 °C reactor temperature (**b**), 10 °C condenser temperature (**c**).

It can be observed that a higher temperature within the reactor results in an elevated conversion rate, and that a low condenser temperature has a similar effect. This can be clearly related to a larger pressure difference between the reactor and condenser, which leads to an increased vapour mass flow. The diagrams, which illustrate the effect of temperature on vapour mass flow while maintaining a constant pressure difference, e.g., 500/80 and 470/45 where Δp is 20 kPa and 22 kPa, respectively, demonstrate that the pressure difference is a significant determinant of the flow rate.

3.2.3. Heat Recovery

An examination of the latent heat output as a function of the pressure difference, illustrated in Figure 10, indicates that apart from minor deviations, a linear relationship between these variables exists. This relation appears to be directly coupled to the pressure difference between the reactor and condenser. The results demonstrate that the reactor can be operated in a flexible manner, accommodating a range of conditions. It can thus be concluded that the system could be employed as a heat source for conventional domestic heating systems, as well as for heating networks. From a technical standpoint, operating the reactor at low temperatures (T < 500 °C) is advantageous, as high temperatures necessitate the selection of more robust materials and components, which in turn increases costs. Additionally, lower temperatures reduce the overall energy losses of the system. However, from the perspective of performance optimization, it is preferable to operate at the highest possible pressure difference between the reactor and condenser.

Nevertheless, a comparison of the actual performance with the theoretical potential, based on the kinetics presented by Schaube et al. [5], reveals that the reaction rate is significantly slower than the theoretical kinetics of the reaction. Additionally, the data obtained from the heating wire control indicate that the available heating power is not being utilised efficiently, with the exception of the preheating process. These observations suggest that the reaction is still constrained by material transport, despite the enhanced filtration.

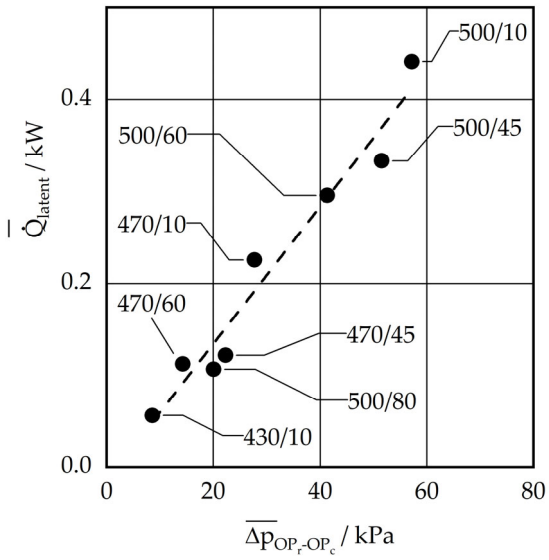

Figure 10. Average latent heat recovered as a function of the pressure difference between the reactor and the condenser for the investigated operating points.

The investigations have revealed potential options for enhancing the system's performance. In general, an increase in mass flow in the direction of the condenser is required in order to achieve a higher power output. In addition to increasing the pressure difference by raising the reactor pressure and/or lowering the condensation temperature, this can be achieved by further reducing the pressure resistance. One method of achieving this is by increasing the filter area. The installation of an additional filter surface on the flange opposite the current one would result in a doubling of the filter area, which may in turn lead to a doubling of the mass flow for identical reaction conditions. Modifying the reactor configuration to a shorter reactor chamber with a larger diameter or utilising the jacket surface as a filtration surface would also increase the filtration area and, consequently, the mass flow. However, it is essential to ensure that an adequate energy transfer from the surface to the material is maintained and that the formation of deposits on the filter surface is prevented. In addition to increasing the filter area, reducing the deposit thickness on the filter surface could be an additional approach to achieve higher system performance. This would necessitate the cutting edge being placed closer to the filter surface.

3.2.4. Permeability of Filter Cake Formation

The characteristics of the filter deposits are a significant factor in the design and future development of the technology. As part of the investigation, the permeability of the 3 mm thick agglomeration layer and the mesh filter was determined. Figure 11 illustrates the calculated permeability values for tests conducted with a high vapour mass flow rate, namely 500/10, 500/56, and 500/45. For purposes of clarity, the moving average of the values over a five-minute interval is presented. It can be observed that the permeability in the tests assumes constant values within the range of 10^{-13} m^2 to 10^{-12} m^2. This corresponds to the values measured by Gollsch et al. [4] under laboratory conditions. However, it is notable that reducing the thickness from 3 mm to 1.5 mm would result in a comparable effect to that of doubling the filter surface.

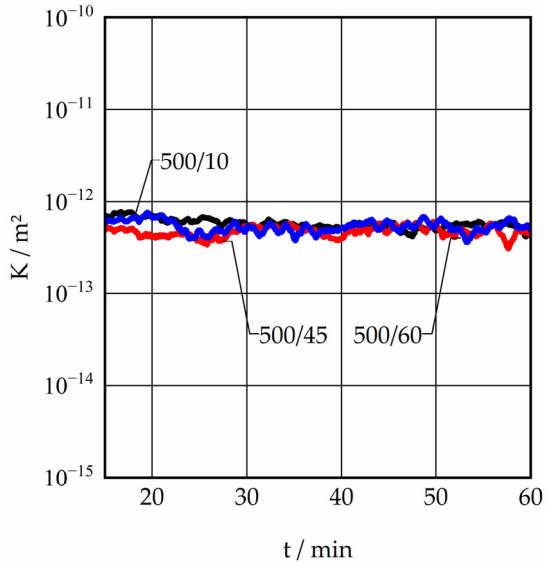

Figure 11. Measured permeability values for different operating conditions for a 3 mm filter cake formation.

4. Conclusions

The thermal energy contained in the water vapour that is released during the charging reaction of a thermochemical energy storage system based on $Ca(OH)_2$ represents approximately 40% of the required charging energy. It is therefore essential that this thermal energy can be used as useful heat in the application in order to ensure the energy-efficient operation of the storage system. The primary objective of this study was to conduct an experimental investigation and demonstrate the effective recovery of the latent and heat energy produced during the dehydration reaction of $Ca(OH)_2$. The recovery of heat has been demonstrated and quantified successfully at temperatures of 45 °C, 60 °C, and 80 °C. Based on the experimental verification, it can be concluded that the utilisation of this energy is feasible in applications such as district heating networks or residential hot water production, with the option of adjusting the temperature level to suit specific requirements. Furthermore, the reactor operation demonstrated that the adjustment of reaction and recovery temperature defines a potential pressure difference between the reactor and condenser. It can be postulated that higher recovery temperatures, such as 150 °C or 200 °C, would also be feasible. The reactor power presented only includes the latent heat of the water vapour that is a by-product of the energy-storing process, which according to Schmidt et al. [10] accounts for approx. 24% of the reactor power. The power of thermochemical energy storage can be assumed to be approximately twice as high. The utilisation of the technology for seasonal energy storage for domestic applications is feasible after an upscaling of the reactor, and the combination with common heat pumps is also quite conceivable, see Weber et al. [21]. For industrial applications as a system-relevant technology in heating networks for heat supply or electricity grids as a peak shaving technology or seasonal energy storage, a significant increase in the specific energy density of the system is required, which goes hand in hand with a significant improvement in the water vapour transport.

For further development it is sufficient to consider the pressure difference resulting from the operating temperatures and related gas velocities in the reactor design. The presented data, in conjunction with the existing thermodynamic and kinetic data, now enables the simulation of application-oriented reactor operation strategies and the extraction of reactor design constraints from the models. At the system level, the operation and integration of the storage reactor in larger energy networks can now be simulated, allowing for the analysis of the energetic and economic value of the storage system.

Furthermore, the operation of the reactor enabled the identification of significant factors pertaining to mass transfer in a mechanically fluidised bed reactor concept. It can be concluded that the filtration of gas and particles represents a significant challenge within

the context of the current reactor design. The fluidisation of the particles within the reaction chamber results in their instantaneous movement in the direction of the gas flow as soon as a gas stream exits the reactor. This results in an immediate and dense clogging of the filter, which in turn causes a significant pressure drop in the filter cake. The implementation of a rotating cutting tool within the design enables the continuous cleansing of the filter throughout the operational period, thereby limiting the overall thickness of the filter cake. The enhanced gas transport resulted in a six-fold increase in performance compared to the operation without a continuously rotating cutting tool in front of the filter. Nevertheless, the findings indicated that the reactor performance remains significantly constrained by the slow mass transfer out of the reactor, which is caused by the pressure drop over the filter cake. The utilisation of rotary components in mixers and reactors is a common practice in the industrial processing of powder materials. However, depending on the design, the components may require frequent maintenance to ensure optimal functionality. It can be concluded that in general, filtration of gas and particles in a mechanically fluidised bed requires a further optimised solution. The experimental data obtained in this work can now be analysed by simulation of the gas transport in the reactor. One approach to optimising the filtration process is to enlarge the filter surface area and simultaneously reduce the thickness of the filter cake layer. Another potential direction for further research could be the specific deceleration of the gas velocity before the filter surface through a corresponding reactor design, for example, changes of the cross section at the gas outlet.

Author Contributions: Conceptualization, V.K., M.L. and M.S.; methodology, V.K. and M.S.; formal analysis, V.K.; investigation, V.K.; writing—original draft preparation, V.K.; writing—review and editing, M.L. and M.S.; visualization, V.K.; supervision, M.L. and M.S. All authors have read and agreed to the published version of the manuscript.

Funding: This work was partially funded by Deutsche Forschungsgemeinschaft (DFG, German Research Foundation) Project-ID 279064222 in the frame of the SFB 1244, A05.

Data Availability Statement: The original contributions presented in the study are included in the article, further inquiries can be directed to the corresponding author.

Acknowledgments: The authors thank Andreas Weigl for his technical support in the preparation of the test bench, as well as Rheinkalk GmbH (Lhoist group) for providing the bulk material.

Conflicts of Interest: The authors declare no conflicts of interest.

Nomenclature

abs	absolute
$A_{condenser}$	condenser water level surface
A_{filter}	filter surface
c	condenser
d_{50}	mean particle diameter
EQ	equilibrium
E_w	equilibrium water pressure
F	filling level
H	enthalpy
ΔH_{vap}	vaporization enthalpy
K	permeability
l	length
M	molar mass
m	mass
MP	multipoint
ρ	density
η	dynamic viscosity

n	amount of substance
OP	operating point
p	pressure
p_c	condenser unit pressure
p_{EQ}	equilibrium pressure
p_r	reactor pressure
$\dot{Q}$	heat flux
r	reactor
T	temperature
t	time
TGA	thermogravimetric analysis
T_{EQ}	equilibrium temperature
$\dot{V}$	volume flow
v	valve
X	conversion
Ø	diameter

References

1. Eurostat. Energy Consumption in Households Statistics Explained. 2021. Available online: https://ec.europa.eu/eurostat/statistics-explained/index.php?title=Energy_consumption_in_households (accessed on 21 June 2024).
2. Eurostat. Electricity Production Capacities for Renewables and Wastes. 2024. Available online: https://ec.europa.eu/eurostat/databrowser/view/NRG_INF_EPCRW__custom_2848440/bookmark/table?lang=de&bookmarkId=7be464f4-0457-45f9-a467-da83849cafeb (accessed on 10 September 2024). [CrossRef]
3. Bao, H.; Ma, Z. 28—Thermochemical energy storage. In *Storing Energy*, 2nd ed.; Letcher, T.M., Ed.; Elsevier: Amsterdam, The Netherlands, 2022; pp. 651–683. [CrossRef]
4. Gollsch, M.; Linder, M. Influence of structural changes on gas transport properties of a cycled $CaO/Ca(OH)_2$ powder bulk for thermochemical energy storage. *J. Energy Storage* **2023**, *73*, 108790. [CrossRef]
5. Schaube, F.; Koch, L.; Wörner, A.; Müller-Steinhagen, H. A thermodynamic and kinetic study of the de- and rehydration of $Ca(OH)_2$ at high HO partial pressures for thermo-chemical heat storage. *Thermochim. Acta* **2012**, *538*, 9–20. [CrossRef]
6. Mejia, A.C.; Afflerbach, S.; Linder, M.; Schmidt, M. Experimental analysis of encapsulated $CaO/Ca(OH)_2$ granules as thermochemical storage in a novel moving bed reactor. *Appl. Therm. Eng.* **2020**, *169*, 114961. [CrossRef]
7. Feng, Y.P.; Li, X.H.; Wu, H.W.; Li, C.R.; Zhang, M.; Yang, H.R. Critical Review of $Ca(OH)_2/CaO$ Thermochemical Energy Storage Materials. *Energies* **2023**, *16*, 3019. [CrossRef]
8. Risthaus, K.; Bürger, I.; Linder, M.; Schmidt, M. Numerical analysis of the hydration of calcium oxide in a fixed bed reactor based on lab-scale experiments. *Appl. Energ.* **2020**, *261*, 114351. [CrossRef]
9. Rentz, A.; Kühl, V.; Sourmelis, T.V.E.; Schmidt, M.; Linder, M.; Sawodny, O.; Böhm, M. Modeling and identification of the hydration process in a $CaO/Ca(OH)_2$-based heat storage system. *Autom* **2023**, *71*, 584–598. [CrossRef]
10. Schmidt, M.; Linder, M. A Novel Thermochemical Long Term Storage Concept: Balance of Renewable Electricity and Heat Demand in Buildings. *Front Energy Res.* **2020**, *8*, 137. [CrossRef]
11. Castilla, G.M.; Guío-Pérez, D.C.; Papadokonstantakis, S.; Pallarès, D.; Johnsson, F. Techno-Economic Assessment of Calcium Looping for Thermochemical Energy Storage with CO Capture. *Energies* **2021**, *14*, 3211. [CrossRef]
12. Wang, K.; Yan, T.; Li, R.; Pan, W. A review for $Ca(OH)_2/CaO$ thermochemical energy storage systems. *J. Energy Storage* **2022**, *50*, 104612. [CrossRef]
13. Mejia, A.C.; Afflerbach, S.; Linder, M.; Schmidt, M. Development of a Moving Bed Reactor for Thermochemical Heat Storage Based on Granulated $Ca(OH)_2$. *Processes* **2022**, *10*, 1680. [CrossRef]
14. Fang, Y.; Zhao, J.L.; Zhang, C.X.; Li, Y.J. Exothermic Performance of the Calcined Limestone Determined by Exothermic Temperature under Fluidization during $CaCO_3/CaO$ Energy Storage Cycles. *J. Therm. Sci.* **2023**, *32*, 1784–1796. [CrossRef]
15. Wuerth, M.; Becker, M.; Ostermeier, P.; Gleis, S.; Spliethoff, H. Development of a Continuous Fluidized Bed Reactor for Thermochemical Energy Storage Application. *J. Energy Resour. Technol.* **2019**, *141*, 070710. [CrossRef]
16. Rougé, S.; Criado, Y.A.; Soriano, O.; Abanades, J.C. Continuous $CaO/Ca(OH)_2$ Fluidized Bed Reactor for Energy Storage: First Experimental Results and Reactor Model Validation. *Ind. Eng. Chem. Res.* **2017**, *56*, 844–852. [CrossRef]
17. Risthaus, K.; Linder, M.; Schmidt, M. Experimental investigation of a novel mechanically fluidized bed reactor for thermochemical energy storage with calcium hydroxide/calcium oxide. *Appl. Energ.* **2022**, *315*, 118976. [CrossRef]
18. Abdullah; Koushaeian, M.; Shah, N.A.; Chung, J.D. A review on thermochemical seasonal solar energy storage materials and modeling methods. *Int. J. Air-Cond. Refrig.* **2024**, *32*, 1. [CrossRef]
19. Abedin, A.H.R. A Critical Review of Thermochemical Energy Storage Systems. *Open Renew. Energy J.* **2011**, *4*, 42–46. [CrossRef]

20. Rentz, A.; Böhm, M.; Sawodny, O. Multi-Stage Optimization for Long-Term Building Climate Operation with Seasonal Thermal Storage. In Proceedings of the 2023 IEEE 19th International Conference on Automation Science and Engineering (CASE), Auckland, New Zealand, 26–30 August 2023; pp. 1–6.
21. Weber, S.O.; Oei, M.; Linder, M.; Böhm, M.; Leistner, P.; Sawodny, O. Model predictive approaches for cost-efficient building climate control with seasonal energy storage. *Energ Build.* **2022**, *270*, 112285. [CrossRef]